Journal of Alloys and Compounds 581 (2013) 508–514

Contents lists available at ScienceDirect

Journal of Alloys and Compounds

journal homepage: www.elsevier.com/locate/jalcom

Theoretical study on tetragonal transition metal dinitrides from first principles calculations

Haiyan Yan [a,*], Meiguang Zhang [b], Qun Wei [c,*], Ping Guo [d]

[a] College of Chemistry and Chemical Engineering, Baoji University of Arts and Sciences, Baoji 721013, People's Republic of China
[b] Department of Physics and Information Technology, Baoji University of Arts and Sciences, Baoji 721016, People's Republic of China
[c] School of Science, Xidian University, Xi'an 710071, People's Republic of China
[d] Department of Physics, Northwest University, Xi'an 710069, People's Republic of China

ARTICLE INFO

Article history:
Received 16 May 2013
Received in revised form 22 July 2013
Accepted 23 July 2013
Available online 31 July 2013

Keywords:
First principles calculations
Transition metal ditrinides
Structural stability
Mechanical properties

ABSTRACT

Three new transition metal dinitrides TMN_2 (TM = Ta, W, and Re) with the *P*4/*mbm* structure are investigated by the first principles calculations method based on the density functional theory. The elastic constants and phonons calculations have confirmed that these three compounds are all mechanical and dynamically stable at ambient pressure. The distributions of elastic moduli of these dinitrides have been systematically studied and the obtained results indicate that the (001) plane may be viewed as the cleavage plane for TaN_2 and WN_2 as well as (100) plane for ReN_2. Moreover, TMN_2 within this tetragonal structure are found to be ultra-incompressible and hard, among which WN_2 exhibits the largest bulk modulus (389 GPa) and Vickers hardness (38.5 GPa). Density of states calculation revealed that the strong TM–N covalent bonding is the driving force for the high bulk and shear modulus as well as small Poisson's ratio of the studied dinitrides.

1. Introduction

Transition metal (TM) nitrides have attracted considerable attentions from both theoretical and experimental studies due to their extreme hardness and durability as well as the outstanding mechanical, electronic, magnetic and optoelectronic properties [1–3]. Most of the early transition metal mononitrides are well known hard materials. For example, TiN and CrN hard coatings are widely used in cutting tools industry [4]. Recently, great interest for transition metal nitrides has re-emerged based on the design concept for intrinsically superhard compounds that the interaction of lights elements (e.g., B, C, N, and O) into the transition metal lattices to form strong covalent bonds yet keeping a high valence-electron density and bulk moduli [5,6]. Taking advantage of high-pressure techniques, bulk TM3N4 (TM = Zr, Hf) [3] with high elastic moduli and hardness has been obtained, opening new avenues for the synthesis of other TM nitrides. Subsequently, the platinum-metal (such as Pt, Ir, Os, and Pd) dinitrides were successfully synthesized under high pressure and high temperature (HPHT) [7–10]. The anomalously ultra-high incompressibility of these nitrides (428 GPa for IrN_2), comparable to that of *c*-BN, suggests that they are potential (super)hard materials. These pioneering studies have stimulated considerable research enthusiasm for 5*d* TM nitrides. More recently, a hexagonal MoS_2-type ReN_2 was synthesized by metathesis reaction using X-ray diffraction under high pressure by Kawamura et al. [11]. However, a following theoretical work [12] has revealed that this MoS_2–ReN_2 is mechanical unstable and it is actually nitrogen-vacancies in MoS_2–ReN_2. Strikingly, theoretical calculations for this nitrogen-vacancies phase correctly reproduce the experimental X-ray diffraction pattern. Their further structural searching identifies a possible ground state monoclinic structure and a high-pressure tetragonal phase (space group: *P*4/*mbm*, *Z* = 2) for ReN2. Especially, this *P*4/*mbm*-ReN_2 exhibits an unusual incompressibility along the *c* axis, close to that of diamond.

Up to now, however, TMN_2 (TM = Hf, Ta, and W) have not been synthesized in crystalline form when compared to other 5*d* TMN_2 (TM = Os, Ir, and Pt) compounds. Therefore, many theoretical studies [13–23] have proposed a series of hypotheses on the structures and properties of TMN_2 (TM = Hf, Ta, and W). Recently, HfN_2 and TaN_2 within four different structures fluorite-type, pyrite-type, $P6_3/mmc$, and $P\bar{6}m2$ structures have been systematically studied [13–15], and these two compounds within pyrite-type structure are potential ultra-incompressible. For WN_2, Wang et al. predicted [16] two types of hexagonal structures which are ultra-incompressible and are energetically superior to the previously proposed cotunnite phase [17]. Meanwhile, numerous theoretical studies have proposed different structures for ReN_2 [18–23], among which a tetragonal phase for ReN_2 suggested by Du et al. is potential superhard. Therefore, as a possible metastable phase, the

* Corresponding authors. Tel./fax: +86 917 3566589.
E-mail addresses: hyyan1102@163.com (H. Yan), weiaqun@163.com (Q. Wei).

0925-8388/$ - see front matter Crown Copyright © 2013 Published by Elsevier B.V. All rights reserved.
http://dx.doi.org/10.1016/j.jallcom.2013.07.157

*P*4/*mbm*-ReN_2-type structure mentioned above can be extended by those of Hf, Ta, and W which can provide further details are highly desirable. However, the calculated phonon dispersion curves in the present work indicate that only TaN_2 and WN_2 with the *P*4/*mbm* structure are dynamically stable. Accordingly, to explore such possibilities and provide guidance for future experimental efforts, here we perform first principles density functional theory (DFT) calculations to investigate the structural stability, mechanical properties, electronic properties, and chemical bonding of TaN_2 and WN_2 in comparison with ReN_2. The calculated results indicate that these dinitrides are mechanically stable and exhibit excellent mechanical properties. We hope our results can stimulate further experimental research to synthesize these ultra-incompressible and potential (super)hard compounds.

2. Computational methods

The DFT calculations have been performed within generalized gradient approximation (GGA) [24], as implemented in the Vienna *ab initio* simulation package (VASP) [25]. The electron and core interactions were included by using the frozen-core all-electron projector augmented wave (PAW) potential [26] of the metal atoms including *d* electrons as valence states. The integration in the Brillouin zone was employed using the Monkhorst–Pack scheme [27] with a grid of 0.03 $Å^{-1}$, an energy cutoff of 800 eV, and a tetrahedron method with Blöchl corrections for the energy calculation and Gaussian smearing for the stress calculations. During the structural optimizations, all forces on atoms were converged to the order of 0.001 eV/Å, and the external stresses were reduced to be less than 0.01 GPa. The phonon calculations were carried out by using a supercell approach as implemented in the PHONOPY code [28]. Single crystal elastic constants were calculated from evaluation of stress tensor generated small strain, and the bulk modulus, shear modulus, Young's modulus, and Poisson's ratio were thus derived from the Voigt–Reuss–Hill approximation [29].

3. Results and discussion

The considered *P*4/*mbm* crystal structure of TMN_2 is shown in Fig. 1. It can be seen that this *P*4/*mbm* phase consists of a fundamental building block connected by edge along the *c*-axis: a tetragonal sublattice (solid line cell in Fig. 1) which can be viewed as a distorted CsCl-type structure. Table 1 lists the calculated lattice constants, equilibrium volumes, bond lengths, bulk moduli, and their pressure derivatives of TMN_2 (TM = Ta, W, and Re) along with previous theoretical values of ReN_2 [12]. The bulk moduli and their pressure derivatives are obtained by fitting pressures and cell volumes with the third-order Birch–Murnaghan equation of state (EOS) [30]. From this table, the calculated lattice parameters, equilibrium volumes and bond lengths of ReN_2 are in good agreement with previous theoretical results. However, for other compounds of TaN_2 and WN_2, there are no available experimental data and theoretical values for comparison. Therefore, the present results could provide useful information for further experimental or theoretical investigations. Moreover, as in the Birch–Murnaghan EOS treatment, we also obtained the values of equilibrium bulk moduli and their pressure derivatives for these three dinitrides presented in Table 1. It can be seen that these compounds possess a large value of bulk moduli which are comparable to those of synthesized platinum-metal dinitrides (PtN_2: 372 GPa [7], OsN_2: 358 GPa [9], IrN_2: 428 GPa [9]), but larger than previous proposed structures of TaN_2 [13,14], WN_2 [16], and ReN_2 [18–20]. Thus, one might expect their excellent ultra-incompressibility. At zero-temperature a stable crystalline structure requires all phonon frequencies to be positive. Therefore, we have performed the full phonon dispersion calculations for TMN_2 (TM = Ta, W, and Re) at 0 GPa. As shown in Fig. 2, no imaginary phonon frequency was detected in the whole Brillouin zone, indicating the dynamical stability of the TaN_2, WN_2, and ReN_2, respectively. It is important to explore the thermodynamic stability of TMN_2 with *P*4/*mbm* structure for further experimental synthesis. The thermodynamic stability at ambient pressure with respect to decomposition is quantified in terms of the formation enthalpy, using $\Delta H_f = H_{(TMN_2)} - H_{(TM)} - H_{(N_2)}$. The ΔH_f is the formation enthalpy, the body-centered-cubic Ta and W (space group: *Im*-3*m*), hexagonal Re (space group: $P6_3/mmc$), and α-phase N_2 are chosen as the reference phases. The calculated ΔH_f per formula unit (f.u.) of these compounds are listed in Table 1, together with other theoretical values for WN_2. Compared to the negative formation enthalpy values of previous candidates $P6_3/mmc$ [16], $P\bar{6}m2$ [16], and $P2_1/c$ [22], the *P*4/*mbm*-WN_2 is metastable with positive formation enthalpy comparable to that of *P*4/*mmm* phase proposed by Du et al. [20]. Therefore, high temperatures are needed to synthesize this *P*4/*mbm* structure for WN_2 in actual experiment. Results obtained by this reaction route for TaN_2, on the contrary, have demonstrated its stability against the decomposition into the mixture of Ta and N_2, suggesting that it is most likely to be synthesized at ambient pressure.

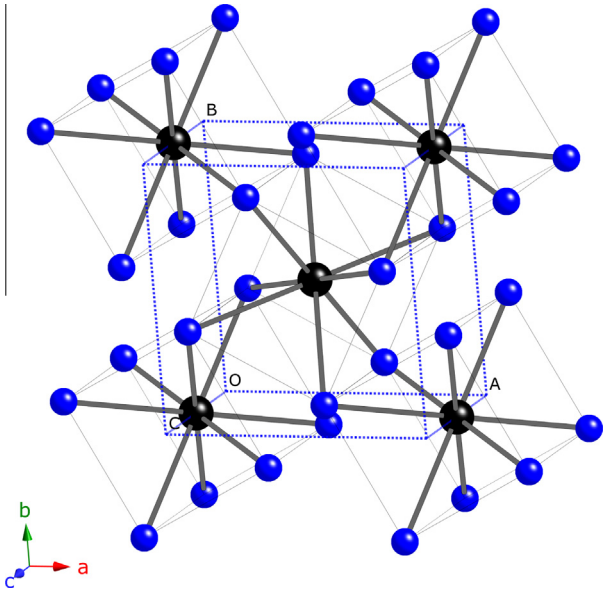

Fig. 1. Crystal structure of the tetragonal *P*4/*mbm* phase. The black and blue spheres represent TM and N atoms, respectively. (For interpretation of the references to color in this figure legend, the reader is referred to the web version of this article.)

In order to provide some insights into the pressure behavior of TMN_2, the pressure acting on the system as functions of lattice parameters (a/a_0 and c/c_0) and unit cell volume (V/V_0) are plotted in Fig. 3, where a_0, c_0, and V_0 are the equilibrium structural parameters at zero pressure. The structural behaviors of synthesized hexagonal Re_2N and Re_3N as well as *c*-BN under pressure were also presented in Fig. 3 for comparison. Firstly, it can be seen that the incompressibility along the *c*-axis is larger than that along the *a*-axis for each TMN_2 compound, suggesting their clear elastic anisotropy. The incompressibility of WN_2 is almost identical to that of ReN_2, but larger than that of TaN_2. Secondly, both WN_2 and ReN_2 exhibit a larger *a*-axis incompressibility and similar volume incompressibility when compared to recently synthesized ultra-incompressible Re_2N and Re_3N. Thirdly, we notice that the volume incompressibility of WN_2 and ReN_2 exceeds that of *c*-BN at high pressure, although *c*-BN has the higher bulk at zero pressure. Take WN_2 for example, by fitting obtained data with least squares meth-

Table 1
Calculated equilibrium lattice constants a_0 (Å), c_0 (Å), equilibrium volume V_0 (Å^3), bond length (Å), EOS fitted bulk modulus B_0 (GPa), its pressure derivative B_0', and formation enthalpy ΔH_f (eV/f.u.) for the $P4/mbm$-TMN_2, respectively.

TMN_2	Space group	a_0	b_0	c_0	V_0	d_{TM-N}	d_{N-N}	B_0	B_0'	ΔH_f
TaN_2	$P4/mbm$	4.403		2.839	55.041	2.272	1.410	343	4.477	−0.951
WN_2	$P4/mbm$	4.331		2.761	51.784	2.221	1.408	390	4.590	0.537
	$P6_3/mmc$[a]	2.934		7.790	58.07	2.102	1.405			−0.942
	$P\bar{6}m2$[a]	2.928		3.916	29.069	2.101	1.420			−0.941
	$P4/mmm$[b]	2.71		7.38	54.20	2.23	1.41	378	4.58	0.74
	$P21/c$[c]	4.83	4.88	5.10						−2.67
ReN_2	$P4/mbm$	4.390		2.663	51.330	2.211	1.424	387	4.766	1.938
	$P4/mbm$[d]	4.390		2.644	50.955	2.20	1.453			

[a] Ref. [16].
[b] Ref. [20].
[c] Ref. [22].
[d] Ref. [12].

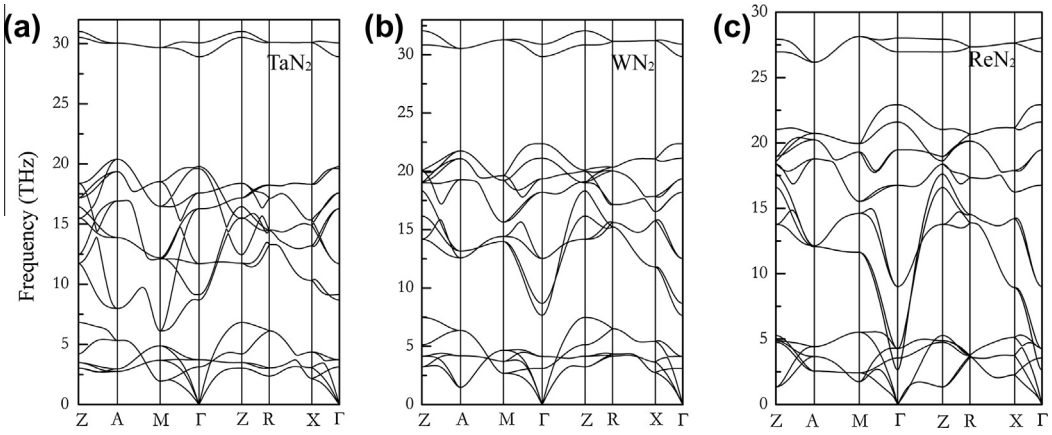

Fig. 2. Phonon dispersion curves of TaN_2 (a), WN_2 (b), and ReN_2 (c) within $P4/mbm$ structure at 0 GPa.

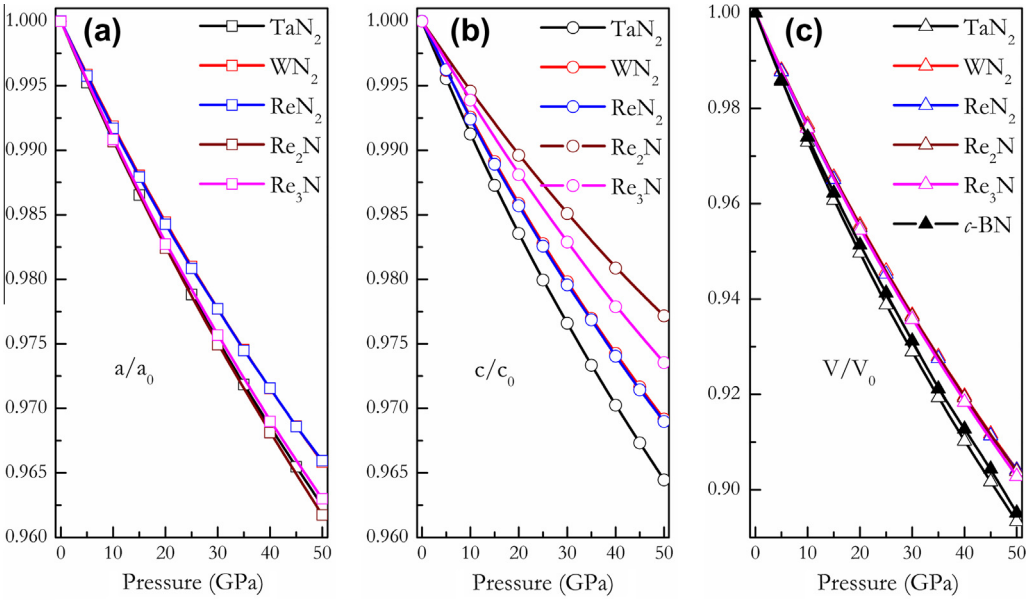

Fig. 3. Calculated a-axis compressions (a/a_0) (a), c-axis compressions (c/c_0) (b), and volume compressions (V/V_0) (c) as a function of pressure TMN_2, respectively.

od, we obtained their relationships at the temperature of 0 K as the following relations:

$$a/a_0 = 0.9995 - 8.36028 \times 10^{-4}P + 3.10152 \times 10^{-6}P^2 \quad (1)$$

$$c/c_0 = 0.99992 - 7.58873 \times 10^{-4}P + 2.90318 \times 10^{-6}P^2 \quad (2)$$

$$V/V_0 = 0.99981 - 2.41 \times 10^{-3}P + 1.00029 \times 10^{-5}P^2 \quad (3)$$

The mechanical properties (elastic constants and elastic moduli) are essential for understanding the macroscopic mechanical properties of solids and for the design of (super)hard materials and their potential technological applications. We calculated the zero-pressure elastic constants C_{ij} of these TMN_2 compounds by the strain–stress method. A small finite strain was applied on the optimized structure and the atomic positions were fully optimized. Then, the elastic constants were obtained from the stress of the strained structure. The calculated elastic constants C_{ij} are listed in Table 2, along with the previous theoretical values of the TMN_2 (TM = Ta, W, and Re) [12–13,16,18–20,22]. It is well known that the elastic stability is a necessary condition for a stable crystal. A tetragonal crystal has to obey the following restrictions of its elastic constants [31]: $C_{11} > 0$, $C_{33} > 0$, $C_{44} > 0$, $C_{66} > 0$, $(C_{11} - C_{12}) > 0$, $(C_{11} + C_{33} - 2C_{13}) > 0$, and $2(C_{11} + C_{12}) + C_{33} + 4C_{13} > 0$. As shown in Table I, these conditions are clearly satisfied for tetragonal stability, confirming that these compounds are mechanically stable. It also can be seen that these compounds possess a remarkable value of C_{33}, especially for WN_2 (894 GPa), which is comparable to those of $P6_3/mmc$ and $P\bar{6}m2$ phases and smaller than that of diamond (1079 GPa) [32]. These results indicate that their *c*-axis directions are extremely stiff. Elastic constant C_{44} is an important parameter of the material's indentation hardness. Among the three compounds within $P4/mbm$ structure and previous proposed candidates, the C_{44} of WN_2 (275 GPa) is the largest one which is close to that of superhard material ReB_2 (276 GPa) [33], indicating that WN_2 has the strong resistance to shear stress. The shear anisotropic factors of the tetragonal $TaN_2/WN_2/ReN_2$ deduced from the present results are $A_1 = 4C_{44}/(C_{11} + C_{33} - 2C_{13}) = 0.70/0.82/0.75$ within (1 0 0) planes between ⟨0 1 1⟩ and ⟨0 1 0⟩ directions, $A_2 = 2C_{66}/(C_{11} - C_{12}) = 0.97/1.03/0.60$ within (0 0 1) shear planes between ⟨1 1 0⟩ and ⟨0 1 0⟩ directions, indicating a certain degree of elastic anisotropy.

Based on the calculated C_{ij}, the corresponding six independent elastic compliance constants s_{ij} of the tetragonal crystal given by Sirdeshmukh were determined [34]. For engineering applications that make use of single crystals, it is necessary to know the values of bulk modulus, Young's modulus, and shear modulus as a function of crystal orientation. As outlined by He et al. [35], executing the appropriate coordinate system transformations for the compliances allows the determination of the variation of Young's moduli E and shear modulus G with crystallographic direction, [*u v w*], for a given crystallographic plane, (*h k l*), containing these directions, i.e., $E_{[uvw]}$ and $G_{(hkl)[uvw]}$ are obtained. For $P4/mbm$ crystal structure, the Young's modulus E can be expressed as:

$$E^{-1} = s_{11}(\alpha^4 + \beta^4) + s_{33}\gamma^4 + 2s_{12}\alpha^2\beta^2 + 2s_{13}(\beta^2\gamma^2 + \alpha^2\gamma^2) + s_{44}(\beta^2\gamma^2 + \alpha^2\gamma^2) + s_{66}\alpha^2\beta^2 \quad (4)$$

where α, β, and γ are the direction cosines of [*u v w*] direction. The three-dimensional surface representations showing the variation of Young's modulus are plotted in Fig. 4. For an isotropic system, one would see a spherical shape. The degree of elastic anisotropy in a system can be directly reflected from the degree of deviation in shape from a sphere. As shown in Fig. 4, all the TMN_2 compounds exhibit the elastic anisotropy since the shape of the Young's modulus representation deviates from a spherical shape, especially for ReN_2 (Fig. 4c). For more detail in Fig. 5, the variation of Young's modulus in the (0 0 1) plane for the quadrant of directions [*u v* w] between [1 0 0] ($\theta = 0^\circ$) and [0 1 0] ($\theta = 90^\circ$). It is clearly seen that Young's moduli of TaN_2 and WN_2 exhibit little change on the whole, on the contrary, ReN_2 possesses a maximum of $E_{[100]} = E_{[010]} = 738$ GPa and a minimum of $E_{[110]} = 533$ GPa. For the (1 0 0) plane in Fig. 5 displays the variation of Young's modulus for directions [0 *v w*] between [0 0 1] ($\theta = 0^\circ$) and [0 1 0] ($\theta = 90^\circ$), the variation tendencies of Young's moduli for TaN_2 and WN_2 are similar among three compounds, with $E_{[001]} = 735/838/764$ GPa and $E_{[011]} = 523/689/630$ GPa for $TaN_2/WN_2/ReN_2$. For $(1\bar{1}0)$ plane, Young's moduli E of TaN_2 and WN_2 behave again very similar for the quadrant of directions [*u u w*] between [0 0 1] and [1 1 0], and the values of $E_{[111]}$ are 520 GPa and 691 GPa for TaN_2 and WN_2, respectively. The Young's moduli E of WN_2 decrease quickly form [0 0 1] to [0 1 0] directions within $(1\bar{1}0)$ plane.

To understand plastic deformations in TMN_2, the dependence of the shear modulus on stress direction is also plotted in Fig. 6. The shear modulus G on the (*h k l*) shear plane with shear stress applied along [*u v w*] direction is given by:

$$G^{-1} = 4s_{11}(\alpha_1^2\alpha_2^2 + \beta_1^2\beta_2^2) + 4s_{33}\gamma_1^2\gamma_2^2 + 8s_{12}\alpha_1\alpha_2\beta_1\beta_2 + s_{66}(\alpha_1\beta_2 + \alpha_2\beta_1)^2 + 8s_{13}(\beta_1\beta_2\gamma_1\gamma_2 + \alpha_1\alpha_2\gamma_1\gamma_2) + s_{44}[(\beta_1\gamma_2 + \beta_2\gamma_1)^2 + (\alpha_1\gamma_2 + \alpha_2\gamma_1)^2] \quad (5)$$

where α_1, β_1, γ_1, α_2, β_2, γ_2 are the direction cosines of the [*u v w*] and [*HKL*] directions in the coordinate systems, where the [*HKL*] denotes

Table 2
Calculated elastic constants C_{ij} (in GPa), isotropic bulk modulus B_H, shear modulus G_H, Young's modulus E_H, and the hardness H_v in unit of GPa for the $P4/mbm$-TMN_2. Also shown are Poisson's ratio υ_H and B_H/G_H ratio.

Crystal	Phases	C_{11}	C_{22}	C_{33}	C_{44}	C_{55}	C_{66}	C_{12}	C_{13}	C_{23}	B_H	G_H	E_H	υ_H	B_H/G_H	H_v
TaN_2	$P4/mbm$	651		771	204		205	228	125		340	225	552	0.2296	1.51	26.3
	Pyrite[a]	255			82			322			299	37				
WN_2	$P4/mbm$	785		894	275		308	188	165		389	300	716	0.1953	1.33	38.5
	$P6_3/mmc$[b]	579		973	233			195	211		364	228				
	$P\bar{6}m2$[b]	588		973	232			191	206		364	231				
	$P4/mmm$[c]	853		861	203		276	122	147		378	295		0.19		
	$P21/c$[d]	537	609	562	137	131	239	214	201	223	332	173				
ReN_2	$P4/mbm$	795		829	240		191	160	176		375	259	632	0.2192	1.45	30.5
	$P4/mbm$[e]	820		967	258		252	165	111		374	297				
	$P4/mmm$[c]	881		936	212		162	134	116		378	295		0.19		
	$Pbcn$[f]	365	553	610	138	230	83	307	232	242	334	127	337	0.3319		
	$Pmmn$[g]	788	889	573	131	339	235	125	308	76	358	238	584	0.23		

[a] Ref. [13].
[b] Ref. [16].
[c] Ref. [20].
[d] Ref. [22].
[e] Ref. [12].
[f] Ref. [19].
[g] Ref. [18].

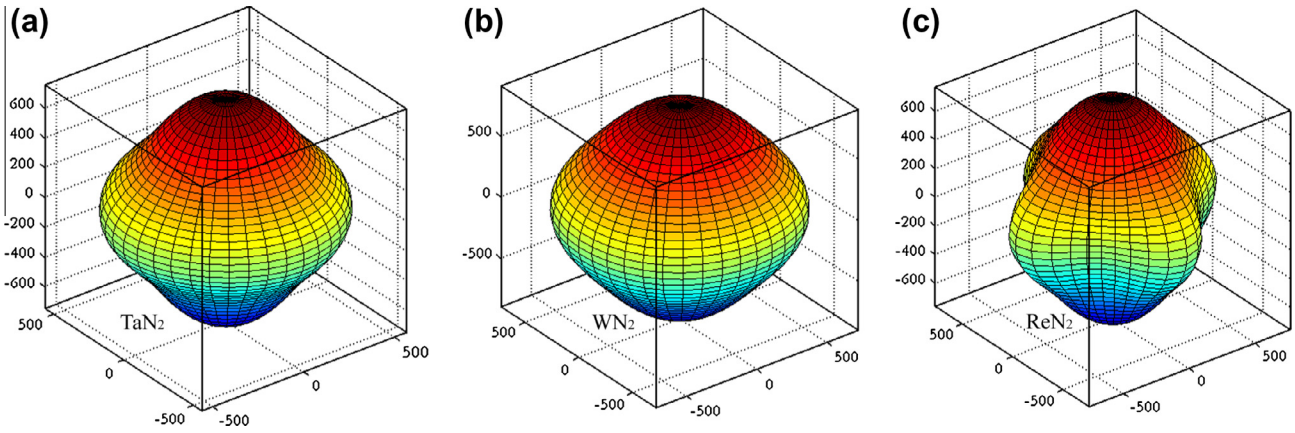

Fig. 4. Three-dimensional surface representations of the Young's modulus for TaN_2 (a), WN_2 (b), and ReN_2 (c).

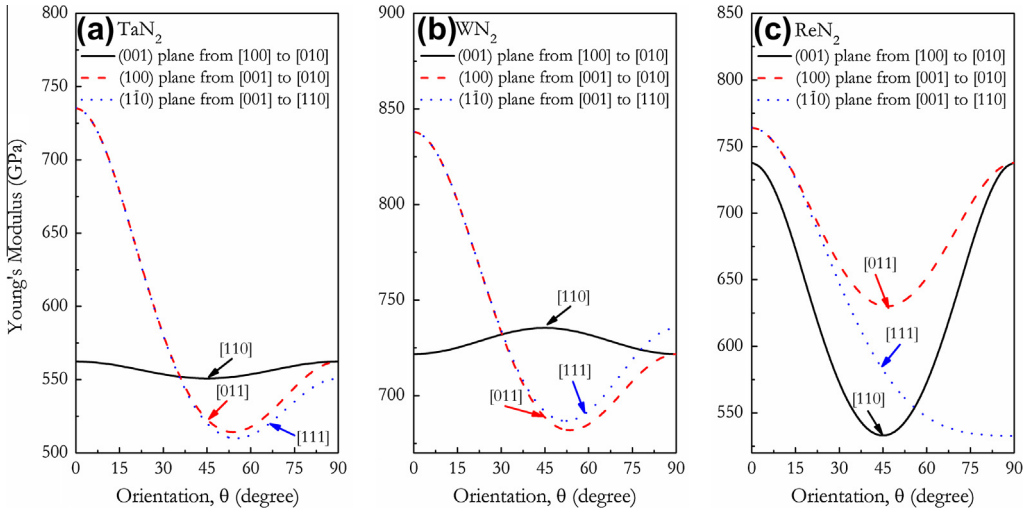

Fig. 5. Orientation dependence of the Young's modulus for TaN_2 (a), WN_2 (b), and ReN_2 (c).

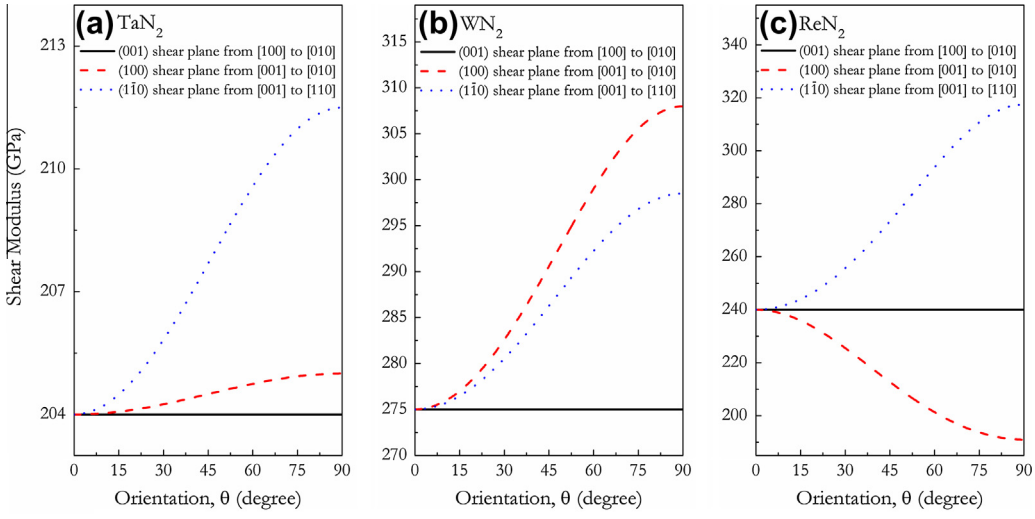

Fig. 6. Orientation dependence of the Shear modulus for TaN_2 (a), WN_2 (b), and ReN_2 (c).

the vector normal to the (hkl) shear plane. For shear plane (001) with the shear stress direction rotated from [100] to [010], the direction cosines are $\alpha_1 = \cos\theta$, $\beta_1 = \sin\theta$, $\gamma_1 = 0$, $\alpha_2 = \beta_2 = 0$, and $\gamma_2 = 1$, where θ is the angle between the [100] and the shear stress direction. By solving Eq. (5), the $G = 1/s_{44} = C_{44}$, which means that within (001) plane, the shear modulus of the TMN_2 is independent

of the shear stress direction. For shear plane (100) with the shear stress directions [0 v w] varying from [100] to [010], the direction cosines are $\alpha_1 = 0$, $\beta_1 = \sin\theta$, $\gamma_1 = \cos\theta$, $\alpha_2 = 1$, $\beta_2 = \gamma_2 = 0$, and $G^{-1} = s_{66} + (s_{44} - s_{66})\cos^2\theta$. Because $s_{44} > s_{66}$ in TaN_2 and WN_2, their shear moduli are the largest along [010] and the smallest along [001]. Contrarily, ReN_2 possesses a maximum of $E_{[001]}$ and a minimum of $E_{[010]}$ due to $s_{44} < s_{66}$. For shear plane $(1\bar{1}0)$ with the shear stress directions [u v w] between [001] and [110] in Fig. 6, the variation tendencies of shear moduli are similar. From Fig. 6, it is clear that the shear moduli are the smallest on the (100) plane for TaN_2, (100) plane for WN_2, and (100) plane for ReN_2, respectively. This means that the (001) plane may be viewed as the cleavage plane for TaN_2 and WN_2 as well as (100) plane for ReN_2.

Based on the calculated elastic constants, the isotropic bulk modulus (B_H) and shear modulus (G_H) for the TMN_2 polycrystalline are calculated by the Voigt–Reuss–Hill approximation [29] in Table 2. The Young's modulus E_H and Poisson's ratio v_H are obtained from the equations of $E_H = 9B_HG_H/(3B_H + G_H)$ and $v_H = (3B_H - 2G_H)/(6B_H + 2G_H)$. The calculated bulk moduli of the TMN_2 are above 340 GPa, indicating ultra-incompressible structural nature. Strikingly, it should be noted that the calculated bulk moduli agree well with those directly obtained from the fitting of the third-order Birch–Murnaghan equation of state (EOS) (see Table 1), which further demonstrates the reliability of our elastic calculations. A material with high bulk modulus is not enough to ensure its high hardness. For the partially covalent transition metal-based materials, the shear modulus of a material quantifies its resistance to the shear deformation and is a better indicator of potential hardness. The value of Poisson's ratio is indicative of the degree of directionality of the covalent bonding, and small Poisson's ratio indicates a strong degree of covalent bonding, which contributes to the materials' hardness. In Table 2, the WN_2 is found to have the highest shear modulus (300 GPa) and lowest Poisson's ratio (0.195), which are two important elastic properties thought to be strongly correlated to hardness. Indeed, the estimated Vickers hardness (H_v) for WN_2 is 38.5 GPa, the largest one among the studied TMN_2 compounds based on the empirical formula for hardness prediction proposed by Chen et al. [36]. Future synthesis of this nitride is thus of great interest and important for utility of this excellent mechanical property. In addition, the ratio between the bulk and the shear modulus B/G are used to predict the brittle or ductile behavior of materials. According to the Pugh criterion [37], the ductile behavior is predicted when $B/G > 1.75$, otherwise the material would fail in a brittle manner. It can be clearly seen in Table 2 that all these TMN_2 compounds are strongly prone to brittle manner.

We have also obtained other fundamental properties using above calculated mechanical quantities. The Debye temperature closely relates to many physical properties of solids, such as specific, dynamic properties, and melting temperature. At low temperature, it can be calculated from the elastic constants using the average sound velocity v_m, by the following equation [38],

$$\Theta_D = \frac{h}{k}\left[\frac{3n}{4\pi}\left(\frac{\rho N_A}{M}\right)\right]^{\frac{1}{3}} v_m \quad (6)$$

where h is Planck's constant, k is Boltzmann's constant, N_A is Avogadro's number, n is the number of atoms per formula unit, M is the molecular mass per formula unit, and ρ is the density. The average sound velocity v_m is given by

$$v_m = \left[\frac{1}{3}\left(\frac{2}{v_t^3} + \frac{1}{v_l^3}\right)\right]^{-\frac{1}{3}} \quad (7)$$

here v_t and v_l are the transverse and longitudinal elastic wave velocities of the polycrystalline materials, which can be obtained using the polycrystalline bulk modulus and shear modulus from Navier's equation [38]. The calculated Debye temperatures of these TMN_2 compounds increase in the following sequence: TaN_2 (666 K) < ReN_2 (697 K) < WN_2 (753 K), which is the same as the trend in estimated hardness of TMN_2 listed Table 2. This can be naturally explained by the empirical linear relationship between hardness and Debye temperature proposed by Abrahams and Hsu [39].

To illustrate the mechanical properties on a fundamental level, the total and site projected electronic densities of states (DOS) of TMN_2 (TM = Ta, W, and Re) at 0 GPa were plotted in Fig. 7, where the vertical dot line is the Fermi level. Clearly, all these structures exhibit metallic behavior by evidence of the finite electronic DOS at the Fermi level (E_F). From the partial DOS, it reveals that the TM-5d orbital has a significant hybridization with N-2p orbital localized in the energy range from −10 eV to 0 eV, indicating the strong TM–N covalent bonding nature. Therefore, the strong covalent Ta–N bond is the main driving force for their high bulk and shear moduli as well as small Poisson's ratio. In addition, the contribution to Fermi level is mainly due to TM-5d orbital which is the principal cause for their metallicity. The typical feature of the total DOS is the presence of so-called pseudogap [40], which is considered as the borderline between the bonding and antibonding states. It can be seen that the E_F of is WN_2 and ReN_2 nearly lying on the pseudogap, respectively, indicating the p-d bonding states started to be saturated. This nearly full occupation of the bonding states enhances the stability of WN_2 and ReN_2. We also performed the Mulliken population analysis of these nitrides and found a charge transfer from TM to N, implying an ionic contribution to the TM–N bonding. We thus conclude that the chemical bonding in these molybdenum borides is a complex mixture of covalent, ionic, and metallic

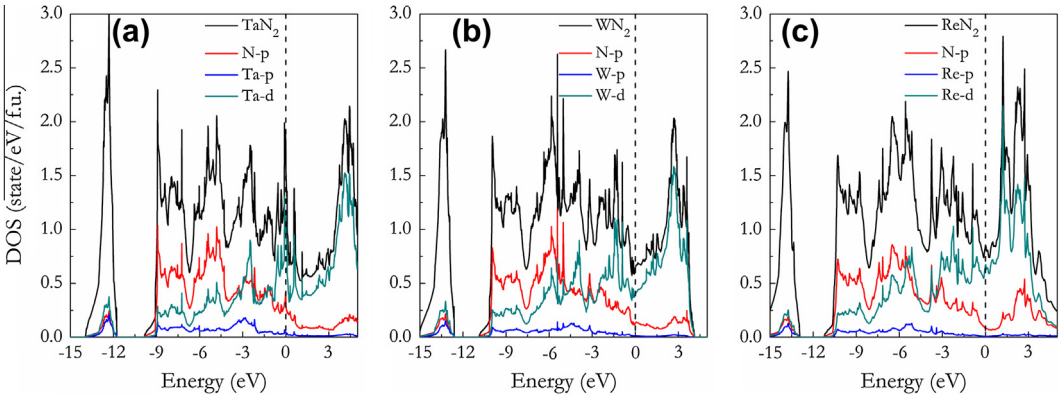

Fig. 7. Total and partial densities of states of TaN_2 (a), WN_2 (b), and ReN_2 (c) at 0 GPa. The vertical dashed line is the Fermi energy.

characters. Such a conclusion was also found in other transition metal nitrides.

4. Conclusions

In summary, by means of density functional theory calculations, we have systematically study the structural stability, mechanical properties, electronic structure and chemical bonding of TMN_2 (TM = Ta, W, and Re) within *P*4/*mbm*-ReN_2 structure. The elastic constants and phonons calculations show that these three compounds are all mechanical and dynamically stable. The Young's modulus and shear modulus as a function of crystal orientation for the TMN_2 were systematically investigated. The results indicate that the (001) plane may be viewed as the cleavage plane for TaN_2 and WN_2 as well as (100) plane for ReN_2. The calculated bulk moduli and hardness suggested that these nitrides are ultra-incompressible and hard materials. The electronic densities of states analysis have demonstrated that the strong covalent TM–N bonding plays a key role in the ultra-incompressibility and hardness of the TMN_2.These findings will inevitably stimulate extensive experimental works on synthesizing these technologically important materials.

Acknowledgments

This work was supported by the Natural Science Foundation of China (No. 11204007), Natural Science Basic Research plan in Shaanxi Province of China (Grant No. 2012JQ1005), Education Committee Natural Science Foundation in Shaanxi Province of China (Grant No. 2013JK0638), and the Fundamental Research Funds for the Central Universities.

References

[1] S.H. Jhi, J. Ihm, S.G. Louie, M.L. Cohen, Nature 399 (1999) 132.
[2] E. Horvath-Bordon, R. Riedel, A. Zerr, P.F. McMillan, G. Auffermann, Y. Prots, W. Bronger, R. Kniep, P. Kroll, Chem. Soc. Rev. 35 (2006) 987.
[3] A. Zerr, G. Miehe, R. Riedel, Nat. Mater. 2 (2003) 185.
[4] R. Buhl, H.K. Pulker, E. Moll, Thin Solid Films 80 (1981) 265.
[5] R.B. Kaner, J.J. Gilman, S.H. Tolbert, Science 308 (2005) 1268.
[6] H.Y. Chung, M.B. Weinberger, J.B. Levine, A. Kavner, J.M. Yang, S.H. Tolbert, R.B. Kaner, Science 316 (2007) 436.
[7] E. Gregoryanz, C. Sanloup, M. Somayazulu, J. Badro, G. Fiquet, H.K. Mao, R.J. Hemley, Nat. Mater. 3 (2004) 294.
[8] J.C. Crowhurst, A.F. Goncharov, B. Sadigh, C.L. Evans, P.G. Morrall, J.L. Ferreira, A.J. Nelson, Science 311 (2006) 1275.
[9] A.F. Young, C. Sanloup, E. Gregoryanz, S. Scandolo, R.J. Hemley, H.K. Mao, Phys. Rev. Lett. 96 (2006) 155501.
[10] J.C. Crowhurst, A.F. Goncharov, B. Sadigh, J.M. Zaug, D. Aberg, Y. Meng, V.B. Prakapenka, J. Mater. Res. 23 (2008) 1.
[11] F. Kawamura, H. Yusa, T. Taniguchi, Appl. Phys. Lett. 100 (2012) 251910.
[12] Y.C. Wang, T.K. Yao, J.L. Yao, J.W. Zhang, H.Y. Gou, Phys. Chem. Chem. Phys. 15 (2013) 183.
[13] J. Zhou, Z.M. Sun, R. Ahuja, J. Alloys Comp. 472 (2009) 425.
[14] S.K.R. Patil, N.S. Mangale, S.V. Khare, S. Marsillac, Thin Solid Films 517 (2008) 824.
[15] G. Soto, Comput. Mater. Sci. 61 (2012) 1.
[16] H. Wang, Q. Li, Y.W. Li, Y. Xu, T. Cui, A.R. Oganov, Y.M. Ma, Phy. Rev. B 79 (2009) 132109.
[17] P. Kroll, T. Schröter, M. Peters, Angew. Chem. Int. Ed. 44 (2005) 4249.
[18] E.J. Zhao, Z.J. Wu, Comput. Mater. Sci. 44 (2008) 531.
[19] Y.L. Li, Z. Zeng, Chem. Phys. Lett. 474 (2009) 93.
[20] X.P. Du, Y.X. Wang, V.C. Lo, Phys. Lett. A 374 (2010) 2569.
[21] H.C. Zhai, X.F. Li, J.Y. Du, Mater. Trans. 53 (2012) 1247.
[22] L. Song, Y.X. Wang, Phys. Status Solidi B 247 (2010) 54.
[23] D.V. Suetin, I.R. Shein, A.L. Ivanovskii, Russ. Chem. Rev. 79 (2010) 611.
[24] J.P. Perdew, K. Burke, M. Ernzerhof, Phys. Rev. Lett. 77 (1996) 3865.
[25] G. Kresse, J. Furthmüller, Phys. Rev. B 54 (1996) 11169.
[26] G. Kresse, D. Joubert, Phys. Rev. B 59 (1999) 1758.
[27] H.J. Monkhorst, J.D. Pack, Phys. Rev. B 13 (1976) 5188.
[28] A. Togo, Phonopy, <http://phonopy.sourceforge.net/>.
[29] R. Hill, Proc. Phys. Soc. London A 65 (1952) 349.
[30] F. Birch, Phys. Rev. 71 (1947) 809.
[31] M. Born, Proc. Cambridge Philos. Soc. 36 (1940) 160.
[32] H.T. McSkimin, P. Andreatch, P. Glynn, J. Appl. Phys. 43 (1972) 985.
[33] M.R. Koehler, V. Keppens, B.C. Sales, R. Jin, D. Mandrus, J. Phys. D: Appl. Phys. 42 (2009) 095414.
[34] D.B. Sirdeshmukh, L. Sirdeshmukh, K.G. Subhadra, Atomistic Properties of Solids, Springer Press, Berlin, 2011.
[35] Y. He, R.B. Schwarz, A. Migliori, J. Mater. Res. 10 (1995) 1187.
[36] X.Q. Chen, H. Niu, D. Li, Y. Li, Intermetallics 19 (2011) 275.
[37] S.F. Pugh, Phil. Mag. 54 (1954) 823.
[38] P. Ravindran, L. Fast, P.A. Korzhavyi, B. Johansson, J. Wills, O. Eriksson, J. Appl. Phys. 84 (1998) 4891.
[39] S.C. Abrahams, F.S.L. Hsu, J. Chem. Phys. 63 (1975) 1162.
[40] P. Vajeeston, P. Ravindran, C. Ravi, R. Asokamani, Phys. Rev. B 63 (2001) 045115.